iScience

CellPress
OPEN ACCESS

Article

Bimetal catalyst based on Fe and Co supported on Al pillared interlayer clays: Preparation, reactivity and mechanism for SCR-CH_4

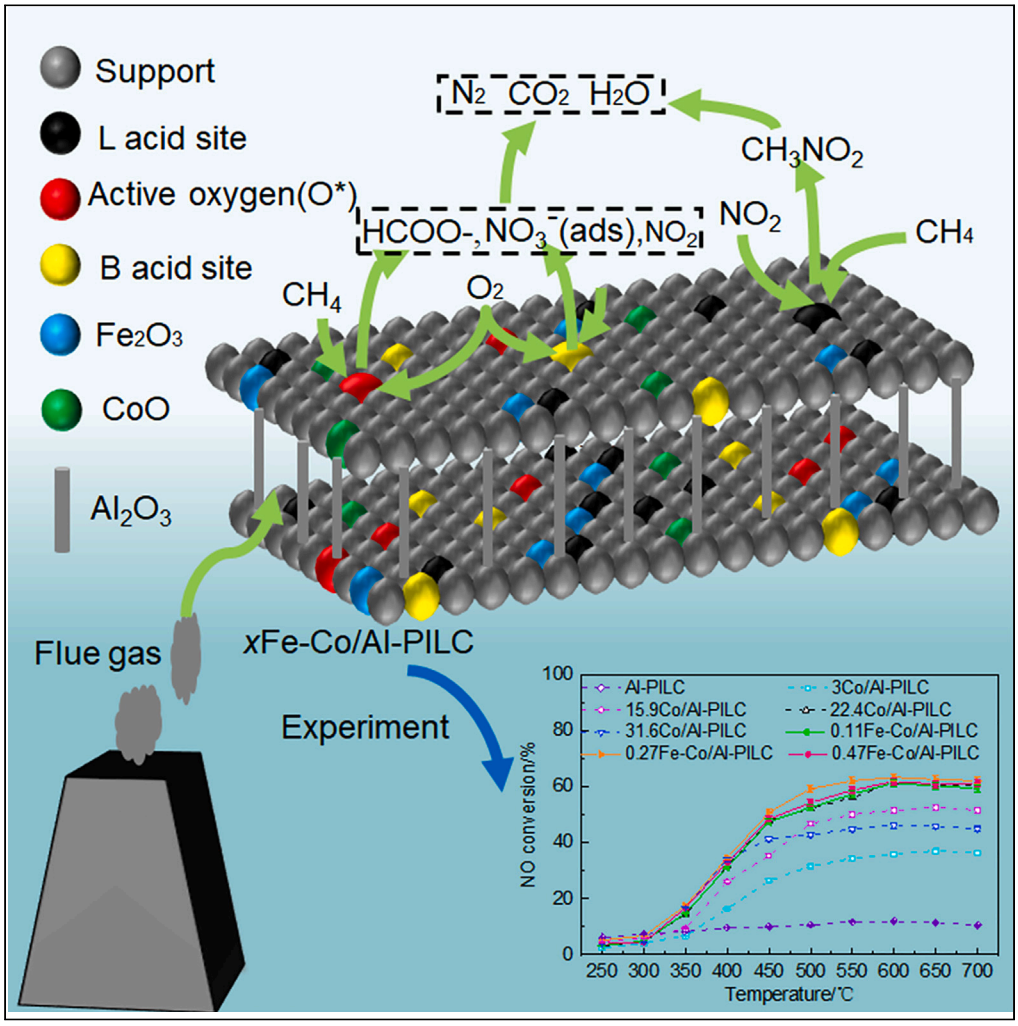

Shuying Ning, Shasha Huang, Honghai Yang, Bingtao Zhao, Yaxin Su

suyx@dhu.edu.cn

Highlights

CH_4-SCR of NO over xFe-Co/Al-PILC catalysts was conducted

Maximum 64% NO removal at 600°C was texted on 0.27 Fe-Co/Al-PILC

Fe significantly improved the resistance to H_2O and SO_2

A preliminary reaction pathway was proposed for CH_4-SCR on 0.27 Fe-Co/Al-PILC

Ning et al., iScience 26, 107432
August 18, 2023
https://doi.org/10.1016/j.isci.2023.107432

iScience

CellPress
OPEN ACCESS

Article

Bimetal catalyst based on Fe and Co supported on Al pillared interlayer clays: Preparation, reactivity and mechanism for SCR-CH_4

Shuying Ning,[1] Shasha Huang,[1] Honghai Yang,[1] Bingtao Zhao,[2] and Yaxin Su[1,3,*]

SUMMARY

Montmorillonite was used as raw clay to prepare the Al-pillared interlayer clay (Al-PILC) as support by impregnation methods. Co and Fe were loaded in series on Al-PILC to prepare the bimetal catalysts (Fe-Co/Al-PILC). The SCR-CH_4 was evaluated in a fixed bed reactor and the results indicated that 0.27Fe-Co/Al-PILC exhibited 100% N_2 selectivity and above 63% NO conversion in the presence of 10% H_2O, and the introduction of Fe significantly improved the Co/Al-PILC catalyst's resistance to H_2O and SO_2. Characterization showed that Lewis and Brønsted acids co-existed on the catalyst surface, and the Lewis acid was the dominant active acid site and enhanced the activation of methane over the 0.27Fe-Co/Al-PILC. Fe promoted the formation of isolated Co^{2+} and CoO species, and the isolated Fe^{3+} particles improved CH_4-SCR performance. The reaction route was proposed based on *in situ* DRIFTS tests and the active intermediates were mainly various nitrates and nitromethane (CH_3NO_2).

INTRODUCTION

Nitrogen oxides (NO_x) from automobile exhaust and stationary sources are major atmospheric pollutants that contribute to ozone depletion, acid rain, and photochemical smog.[1,2] So far, NO_x abatement has become one of the dominant environmental problems.[3] A promising technology for eliminating NO_x is the selective catalytic hydrocarbon reduction of NO_x (HC-SCR).[4] Employing hydrocarbons, e.g., methane, as a reducing agent to reduce NO_x is particularly beneficial for controlling NO_x emissions from natural gas-fired boilers and engines.[5] Moreover, because methane is an unburned compound in the exhaust of stationary sources, the reduction of NO by methane undoubtedly has a broader practical prospect and economic value.[6] Unfortunately, methane is the most stable among hydrocarbons, and its activation is significantly low. The CH_4-SCR activity was usually obviously low over the catalysts with highly active C_2-C_3 hydrocarbons.[7] The catalysts prepared on different carriers also generally suffer from lower denitrification efficiency, weaker water and sulfur resistance, and higher activity temperatures in the CH_4-SCR reaction. Therefore, researching highly active catalysts for CH_4-SCR of NO_x has become a challenging and significant issue.[8]

Currently, diverse types of metals-based catalysts, such as In and Pd, have been used to research the denitrification performance of CH_4-SCR, as shown in Table 1. Although the In-based catalysts can exhibit higher NO conversion, the SO_2 resistance was poor.[9,10] For instance, the In/H-BEA catalyst prepared by impregnating can display NO conversion of 90% in the absence of 200 ppm SO_2 at 450°C, but the NO removal efficiency was less than 55.8% caused by the generation of surface sulfate in the presence of 200 ppm SO_2.[9] Pd metals had poor catalytic activity besides the low economic value in engineering applications. Although the Pd-SBA-Imp sample created using the incipient wetness impregnation technology can exhibit the NO removal of 98% at 300°C, the catalytic activity was low due to the strong interaction between the PdO active species and the silica support.[12]

Table 1 also shows that the $La_{0.8}Sr_{0.2}MnO_3/\alpha Al_2O_3$ catalyst can achieve the optimal CH_4-SCR performance with more than 90% NO removal efficiency at 900°C.[13] However, the activity temperature in the CH_4-SCR reaction of the $La_{0.8}Sr_{0.2}MnO_3/\alpha Al_2O_3$ was significantly high, which was not conducive to the low-temperature activation of methane. In addition, Ga was also reactive during the CH_4-SCR, while

[1]School of Environmental Science and Engineering, Donghua University, Shanghai 201620, China

[2]School of Energy and Power Engineering, University of Shanghai for Science and Technology, Shanghai 200093, China

[3]Lead contact

*Correspondence: suyx@dhu.edu.cn

https://doi.org/10.1016/j.isci.2023.107432

Table 1. The denitrification performance of CH_4-SCR over different catalysts

Catalysts	Feed gas	$DeNO_x$/%	T/°C	Reference
In/H-BEA	600 ppm NO, 600 ppm CH_4, 6%O_2	90	450	Pan et al.[9]
Ru-In/H-SSZ-13	2500 ppm NO, 4000 ppm CH_4, 4%O_2, 6%H_2O	94	550	Yang et al.[10]
Ce/Pd-MOR	0.1%NO, 0.1%CH_4, 7%O_2	35	500	Mendes et al.[11]
Pd-SBA-Imp	150 ppm NO, 1500 ppm CH_4, 7%O_2	98	300	Boutros et al.[12]
$La_{0.8}Sr_{0.2}MnO_3/\alpha Al_2O_3$	1000 ppm NO, 1200 ppm CH_4, 1%O_2	90	900	Teng et al.[13]
5Fe/Ga_2O_3-Al_2O_3	0.1%NO, 0.2%CH_4, 1%O_2, 5%H_2O	60	500	Wen et al.[7]
γ-Ga_2O_3-Al_2O_3	0.1%NO, 0.1%CH_4, 6.7%O_2	90	550	Takahashi et al.[14]
Co/H-MFI	1500 ppm NO, 1500 ppm CH_4, 25000 ppm O_2	20	450	Resini et al.[15]
Co/H-ZSM-5	0.4%NO, 0.4%CH_4, 2%O_2	60	550	Lónyi et al.[16]
In/Co-FER	0.1%NO, 0.2%CH_4, 4%O_2, 0.25%H_2O	97.5	450	Gil et al.[17]
This work	0.1%NO, 0.2%CH_4, 2%O_2, 10%H_2O, 200 ppm SO_2	63%	600	

the removal efficiency was not satisfactory due to the activation of methane in the first step of the SCR reaction was a hardship, e.g., the 5Fe/Ga_2O_3-Al_2O_3 catalyst owned the NO conversion of 60% at 500°C.[7] While the γ-Ga_2O_3-Al_2O_3(ST) catalyst owned the 90% NO removal efficiency at 550°C, the NO conversion was only 50% at 550°C after adding 2.5% H_2O, and that was less than 20% at 500°C under the 5% H_2O atmosphere.[14] Hence, the Ga-based catalyst had the disadvantage of a poor ability to resistance to H_2O. Cobalt metal showed reactivity during CH_4-SCR at medium and high activity temperatures. The NO conversion rate of CH_4-SCR of Co-ZSM-5 and Co-modified H-MOR catalyst can achieve 50% at 500°C and 60% at 550°C, respectively. However, the NO removal efficiency of the In/Co-FER was 97.5% at 450°C in the presence of 0.25% H_2O,[17] but the H_2O content introduced into the flue gas was too little to accurately assess the ability of the In/Co-FER to resist H_2O. In addition, the catalysts based on Co/In/H-ZSM-5 zeolites were studied for CH_4-SCR, and the results showed that the denitration efficiency of the bimetallic catalyst exceeded 60% at 700 K, while the NO conversion rate of the single metal catalyst (Co/H-ZSM-5) was about 20% under the same conditions.[16,18] Water strongly poisoned the Co^{2+} active sites.[16]

The high HC-SCR activity of Fe-based catalysts was due to the excellent redox ability of iron ions between Fe^{2+} and Fe^{3+}, and iron/iron oxides showed excellent resistance to H_2O and SO_2 in the NO removal by CH_4[19,20] Fe or its oxides can significantly improve the NO conversion by light hydrocarbons above 800°C and show intensive resistance to H_2O and SO_2.[20] UV-vis results indicated that the formation of oligomeric Fe_xO_y species enhanced the activation of the catalyst. When Fe/Al PILC is used for C_3H_6-SCR, the sample has excellent resistance to H_2O and SO_2.[21,22]

The Al-PILC (aluminum pillared clay), owning its excellent hydrothermal stability, large specific surface area, and Lewis and Brønsted acids,[23] has been paid attention to for denitrification for C_3H_6-SCR by our group. The structural properties of pillared clay materials could be improved by modifying the preparation and dehydroxylation methods of the pillared metal precursors, where the pillar density determines the ultimate thermal stability of PILC.[24] Alumina cations have certain advantages in increasing the thermal stability of PILC.[25] The pillaring ion Al^{3+} sharply increases the specific surface area of montmorillonite, and a variety of new catalysts were prepared with an ion and metal mixed oxide on an aluminum pillared clay (Al-PILC) support.[26] Much more work is necessary to understand the possible effective catalysts based on PILC supports and other metals.

The development of low-temperature, highly efficient, and low-cost transition metal catalysts with strong resistance to water and SO_2 for CH_4-SCR of NO_x has become a challenging and significant issue. Inspired by the previous literature, we prepared montmorillonite-based Al-pillared clay by impregnation methods, and then Co and Fe were supported on Al-PILC to prepare the bimetallic catalysts for the CH_4-SCR. The catalytic reactivity over Fe-Co/Al-PILC in CH_4-SCR was experimentally investigated as well as the reaction mechanism of NO reduction by methane was preliminarily determined by *in situ* diffuse reflectances Fourier transforms infrared spectrum (*in situ* DRIFTS).

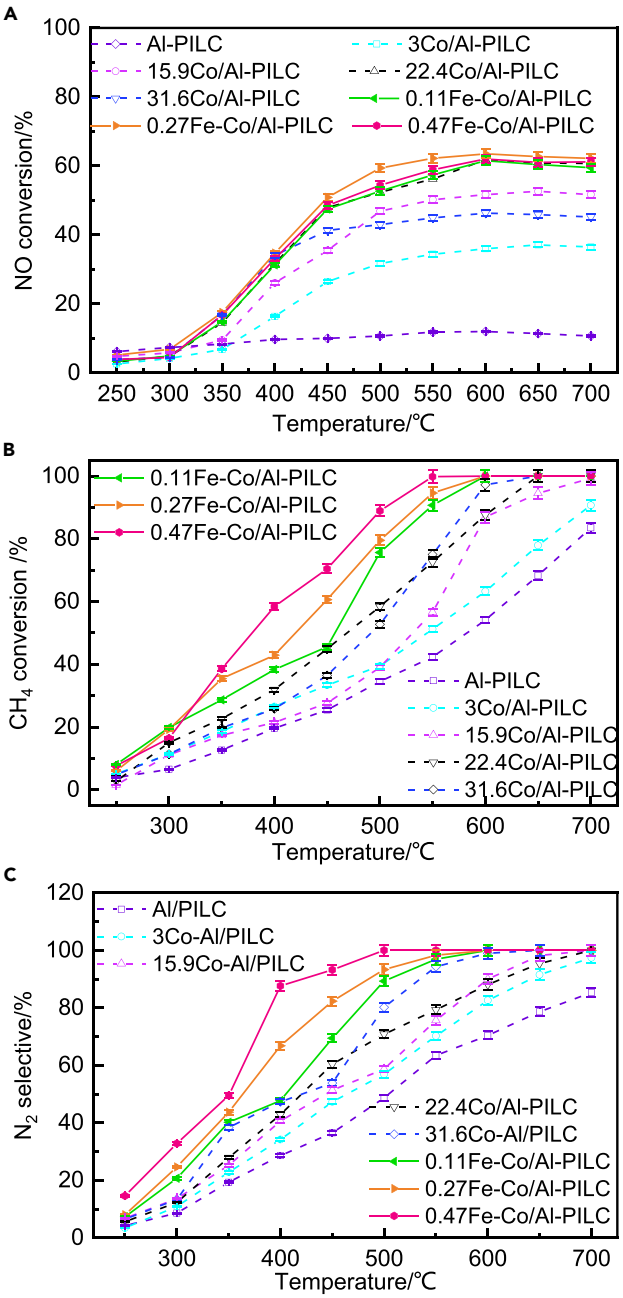

Figure 1. Activity testing of catalysts (conditions: 0.1% NO, 0.2% CH_4, 2% O_2, N_2 balance, GHSV = 14000 h^{-1})

(A) NO conversion.

(B) CH_4 conversion.

(C) N_2 selectivity.

Error bar: −2%–+2%.

RESULTS AND DISCUSSION

Activity testing

Figure 1 exhibits the catalytic activity results of the xFe-Co/Al-PILC catalysts. Figure 1A displays that the NO conversion rosed first with increasing temperature above 300°C and then arrived at a maximum at 600°C, finally slightly declining because of the oxidation of CH_4 by O_2. The NO removal efficiency of the Al-PILC sample remained at about 10% in the region of 400°C–700°C. In contrast, the NO conversion was far more

Table 2. Fe mass, Co mass, textural properties of the catalysts

Catalysts	Fe mass[a] (mg/g)	Co mass[a] (mg/g)	A_{BET}[b] (m^2/g)	volume[c] (cm^3/g)	diameter[d] (nm)
Al-PILC	–	–	86	0.072	14.62
3Co/Al-PILC	–	29.39	98	0.086	9.38
22.4Co/Al-PILC	–	223.93	111	0.109	8.13
31.6Co/Al-PILC	–	315.52	93	0.097	7.26
0.11Fe-Co/Al-PILC	25.4	223.93	124	0.168	3.06
0.27Fe-Co/Al-PILC	60.2	223.93	129	0.264	3.41
0.47Fe-Co/Al-PILC	105.0	223.93	105	0.210	3.40

[a]Metal mass was determined based on the ICP method.
[b]Surface area measured by BET analysis.
[c]Pore volume calculated by the BJH equation.
[d]Pore diameter was calculated according to the BJH equation.

than that of the Al-PILC catalyst after doping Co, indicating that the Co element promoted the NO reduction reactivity for SCR-CH_4. Noteworthily, the NO conversion first increased and then declined as the amount of Co increased, wherein 22.4Co/Al-PILC owned the maximum NO conversion of 62% at 600°C. When the Co-based catalysts were modified by Fe, i.e., the *x*Fe-Co/Al-PILC catalysts, the NO removal efficiency was higher than 22.4Co/Al-PILC. Among all the samples, the 0.27Fe-Co/Al-PILC sample had the highest NO removal efficiency of about 64% at 600°C. It was worth noting that the NO removal efficiency of the 0.47Fe-Co/Al-PILC sample was lower than that of the 0.27Fe-Co/Al-PILC, which was due to Fe_2O_3 particles agglomerating caused the Al-PILC channels generated blocking, which could be proved by the surface area of 0.47Fe-Co/Al-PILC catalyst decreased (listed in Table 2). This result showed that the optimum mass ratio of Fe/Co was approximately 0.27.

In addition, CH_4 conversion increased rapidly and finally became steady shown in Figure 1B. CH_4 was consumed in the progress of NO reduction by methane and the oxidation of CH_4 by oxygen. Compared to other catalysts, the CH_4 conversion value of the 0.47Fe-Co/Al-PILC sample was higher, and the temperature value corresponding to the complete conversion of CH_4 shifts to a lower value, which may be due to excess Fe resulting in more iron oxide, which could contribute to the oxidation of CH_4 by oxygen rather than promote the reaction of CH_4 and NO. N_2 selectivity also indicates catalytic activity performance. The N_2 selectivity rose with increasing temperature before becoming steady, as seen in Figure 1C. Meanwhile, the N_2 selectivity rosed with the amount of Fe increasing and finally remained at 100%. The result could be explained by the drop of Fe being unfavorable for the formation of N_2O and NO_2, improving the N_2 selectivity.[27]

Effect of H_2O and SO_2

The emissions of the combustion of fuel contain water and sulfur dioxide, which affects the activity of the catalyst. For example, introducing 5% water into the NO removal progress over Co-ZSM5 and Co-MOR led to a rapid drop in NO conversion by 20%.[28] NO conversion of CH_4-SCR over the Co-MFI/BEA decreased from 61.9 to 50% after adding 0.078% SO_2.[29] Therefore, the experiment on the influence of existing water and sulfur dioxide on the catalyst performance was conducted separately.

Figure 2A depicts the effect of water on the NO conversion. The conversion of NO for CH_4-SCR over 22.4Co/Al-PILC catalysts significantly decreased by 40% when H_2O (10%) was added, which was ascribed to the preferential adsorption of hydroxyl groups, which was unfavorable for the adsorption of NO or CH_4 over catalysts.[30] However, the removal of NO recovered the original level (more than 63%) when H_2O was absent, demonstrating that the influence of H_2O on the catalyst activity was reversible. Compared to the H_2O resistance of 22.4Co/Al-PILC that of 0.27 Fe-Co/Al-PILC is higher. In addition, the NO conversion rate over 0.27 Fe-Co/Al-PILC only declined by 14% and still kept at about 55% in the presence of H_2O. When shutting down H_2O, the NO conversion rapidly returned to a constant value of around 62%, indicating that the Fe additive improves the H_2O resistance of Fe-Co/Al-PILC.

Figure 2B presents the influence of SO_2 on the catalytic activity over prepared catalysts. It can be seen that the 22.4Co/Al-PILC had a significant drop in NO conversion from 62 to 43% when 0.02% SO_2 was introduced. While there was a slight decrease in the NO conversion of 0.27Fe-Co/Al-PILC catalyst from 64 to

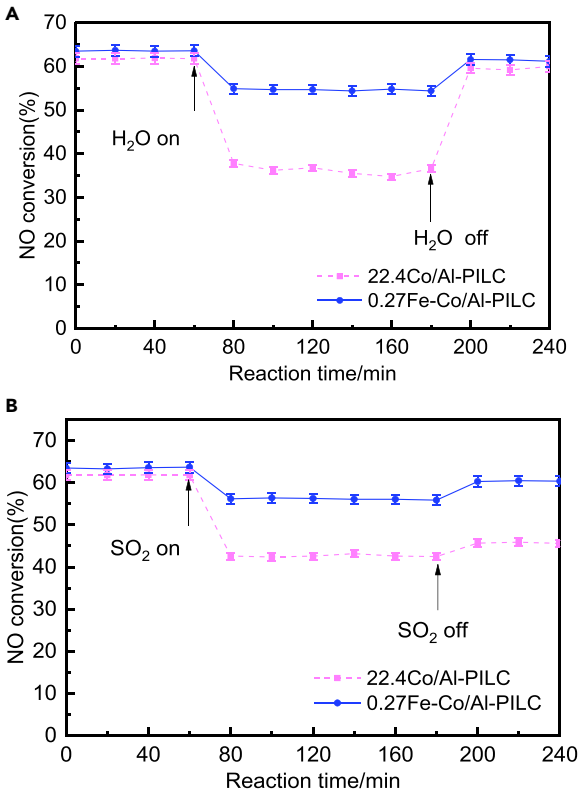

Figure 2. Effects of exiting H_2O and SO_2 on the catalytic activity of catalysts at 600°C

Conditions: NO = 0.1%, CH_4 = 0.2%, O_2 = 2%, 0.02% SO_2 (when used), 10% H_2O (when used), N_2 as balance.

(A) Effects of exiting H_2O on the catalytic activity of 22.4Co/Al-PILC and 0.27Fe-Co/Al- PILC catalysts.

(B) Effects of exiting SO_2 on the catalytic activity of 22.4Co/Al-PILC and 0.27Fe-Co/Al- PILC catalysts.

Error bar: −2%–+2%.

56% after adding 0.02% SO_2, the NO conversion remained around 60% after removing SO_2. This result shows that the Fe additive enhances the SO_2 resistance of the Fe-Co/Al-PILC catalyst.

XRD pattern

The X-ray diffractometer (XRD) spectrum of the original clay (see Figure 3A) exhibited the crystal plane diffraction peak of M (001) at 8.9°, with corresponding layered structure spacing of 1nm. The two-dimensional (*hk*) diffraction peak appeared at 17.8°, 19.75°, and 35.04°, respectively, wherein, the reflection value of 19.75° matched the summation of *hk* indices (02) and (11), and that of 35.04° corresponded to summation over *hk* cues (13) and (20). Moreover, the reflection corresponding to 26.6° and 27.9° were caused by quartz (Q) and silica (C) separately. After introducing the Al element, the diffraction peak matched the crystalline plane M (001) for Al-pillared montmorillonite moved downward to 7.5° resulting in a basal gap of 1.27 nm, suggesting that Al_2O_3 pillars effectively extended the interlayer distance. The intensity of each characteristic peak of Al-PILC was lower than that of the original clay, which may be due to some Al_2O_3 species formed in the process of surface pillaring covering the surface of the carrier, and the other part acts as interlayer pillars to prop up each structural layer. After doping cobalt, the diffraction peak corresponding to Co species was not found in the 3Co/Al-PILC diffraction pattern, which may be due to Co species being highly dispersed on the catalyst surface. With the increase of Co loading, 22.4Co/Al-PILC and 31.6Co/Al-PILC exhibited characteristic diffraction peaks of Co species at 31.3° and 36.6°, corresponding to Co_3O_4 and CoO species, respectively. CoO species could enhance the reduction ability for SCR reaction, which may explain why the *x*Co/Al-PILC catalyst owned higher NO conversion than the Al-PILC catalysts.

Figure 3B shows the XRD patterns. The diffraction peaks at 2θ of 18.84° and 21.68° of the Fe-loaded sample became weaker than that of the 22.4Co-Al-PILC due to the heavy absorption of X-rays by the iron and

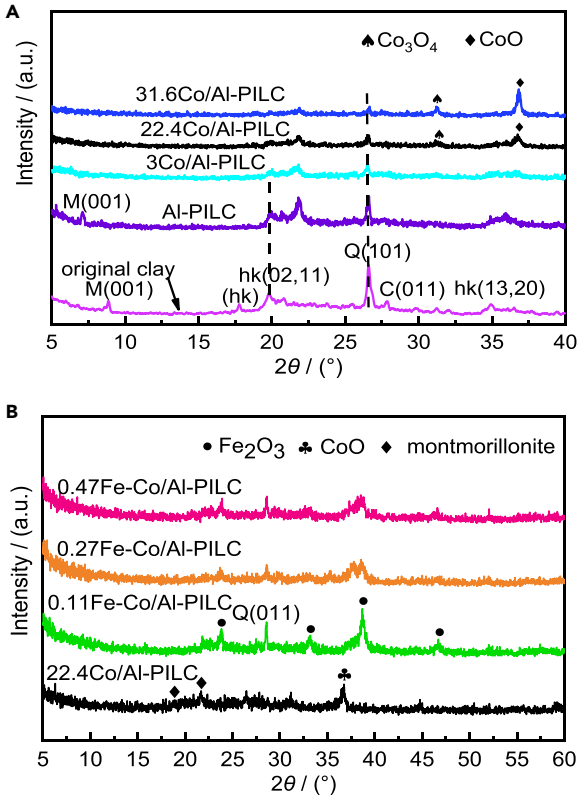

Figure 3. X-ray diffractometer (XRD) spectra of catalysts

(A) XRD spectra of Al-PILC, 3Co/Al-PILC, 22.4Co/Al-PILC, and 31.6Co/Al-PILC catalysts.

(B) XRD spectra of 22.4Co/Al-PILC, 0.11Fe-Co/Al-PILC, 0.27Fe-Co/Al-PILC, and 0.47Fe-Co/Al-PILC catalysts.

cobalt compounds.[31] For the Fe-loaded Fe-Co/Al-PILC catalyst, the diffraction peak intensities of CoO species at 2θ of 36.6° were weakened or even disappeared, which may be due to the introduction of Fe to promote the more uniform dispersion of CoO species on the catalyst surface. The peak intensity of Fe_2O_3 species at 2θ of 23.84°, 33.2°, 38.68°, and 46.7° of 0.27Fe-Co/Al-PILC catalyst was significantly weakened, which may be because it was highly dispersed on the sample surface, providing more active sites and promoting the conversion of NO.[32] The result was consistent with its higher NO conversion in Figure 1A.

N_2 adsorption-desorption

Figure 4 shows the adsorption-desorption of N_2. These isotherms of the prepared samples exhibited type IV with an H3 hysteresis according to the IUPAC,[33] demonstrating that all the samples showed layer structure.[34] In the low relative pressure area (< 0.4), the coincidence of the desorption and adsorption isotherms illustrated that some micropores existed in the catalyst. With the p/p_0 increasing, the adsorption capacity rosed significantly, caused by the capillary conglomeration. The textural characteristics of the prepared catalysts are shown in Table 2. Clearly, after loading Co, the surface area and pore volume increased while the pore diameter reduced. Among the Co-based catalysts, the 22.4Co/Al-PILC catalyst owned a maximum of 111 m^2/g and 0.109 cm^3/g. Compared with the 22.4Co/Al-PILC, the surface area and pore volume of the 33.6Co/Al-PILC reduced to 93 m^2/g and 0.097 cm^3/g, indicating that excess Co species may be occupied the interlayer area. After Fe doping into 22.4Co/Al-PILC, the A_{BET} and pore volume increased, possibly caused by the formation of Fe_2O_3 particles resulting in the distribution of cobalt species as active components.[35] Comparing the series of the *x*Fe-Co/Al-PILC samples implied that with the ferric-cobalt ratio value rising from 0.11 to 0.27, the surface area increased from 124 to 129 $m^2\ g^{-1}$, and the pore volume increased from 0.168 to 0.264 $cm^3\ g^{-1}$. While the ratio of Fe/Co was 0.47, the geometry declined to 105 $m^2\ g^{-1}$ and 0.210 $cm^3\ g^{-1}$, respectively. It was worth noting that the 0.27Fe-Co/Al-PILC had the optimal structure characters when the ratio of Fe/Co was 0.27, indicating that an appropriate ferric-cobalt ratio value can improve the distribution of cobalt species to arrive

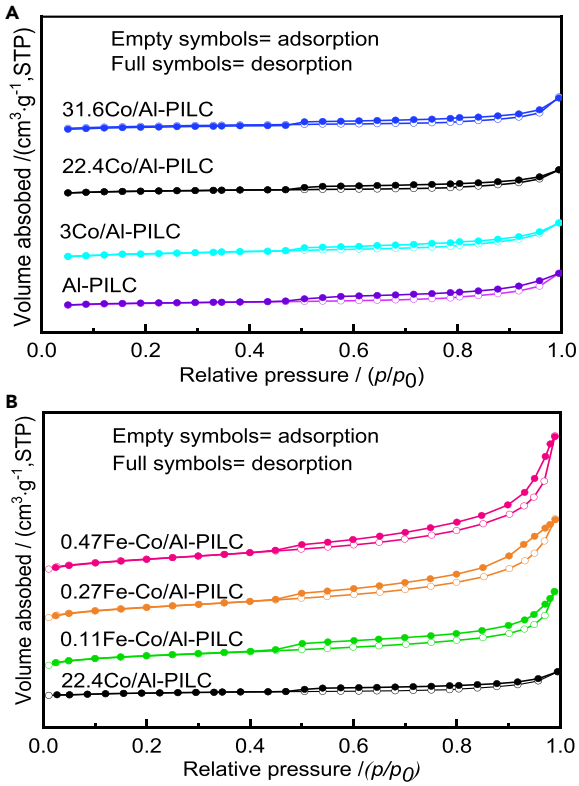

Figure 4. N_2 adsorption-desorption

(A) N_2 adsorption-desorption isotherms of Al-PILC, 3Co/Al-PILC, 22.4Co/Al-PILC, and 31.6Co/Al-PILC catalysts.

(B) N_2 adsorption-desorption isotherms of 22.4Co/Al-PILC, 0.11Fe-Co/Al-PILC, 0.27Fe- Co/Al-PILC, and 0.47Fe-Co/Al-PILC catalysts.

at a larger A_{BET} and pore volume, further resulted in the active species broadly distributed over catalysts to supply more adsorption points for methane. In addition, the doping of Fe decreased the pore diameter, which may be conducive to enhancing the N_2 selectivity.[36]

XPS spectra

X-ray photoelectron spectrum (XPS) tests were used to analyze the chemical states of Co or Fe over catalysts presented in Figure 5. Figure 5A shows that all the Co-based samples exhibited peaks related to Co 2p3/2, Co 2p1/2, and satellites. The core levels of Co 2p3/2 were 780.4 eV, implying that the valence state of Co was +2. Among the Co-based samples, the 22.4Co/Al-PILC owned the maximum of Co^{2+}. Based on the result of Figure 1A, it can be deduced that Co^{2+} was the main active species that caused the 22.4Co/Al-PILC to have the optimal CH_4-SCR performance. In addition, the Co 2p3/2 binding energy of Co^{2+} was higher than the standard binding energy (780.2 eV), indicating that there are different types of Co species in the catalyst, which may exist in the form of CoO, $Co(OH)_2$. The peak near 780 and 781 eV were attributed to Co^{3+} and Co^{2+}, respectively. The binding energy of cobalt shifted (see Figure 5B) after the 22.4Co/Al-PILC catalyst was modified by Fe, demonstrating that the introduction of Fe changed the chemical environments of cobalt. The characteristic peak at 782 eV corresponded to the CoO species. The peak band near 780 eV belonged to Co^{3+}, presenting in Co_3O_4 or oxide-like clusters, and the other near 782 eV belonged to Co^{2+}.[37] As the Fe-Co mass fraction increased, the peak intensity at about 780 eV became stronger. The peak intensity of 782 eV for 0.27Fe-Co/Al-PILC catalyst was the highest among the yFe-Co/Al-PILC samples, demonstrating that the appropriate ratio of Fe to Co was a significant factor that affected the production of Co^{2+}. However, when the content of Fe was excessive, for example, 0.47Fe-Co/Al-PILC, the intensity value at approximately 782 eV changed from strong to weak, implying that an appropriate Fe-Co mass fraction could promote the formation of Co^{2+} attributed to CoO and improve the conversion of NO.[38] The result was consistent with the NO conversion in Figure 1A and the XRD spectrum (Figure 3).

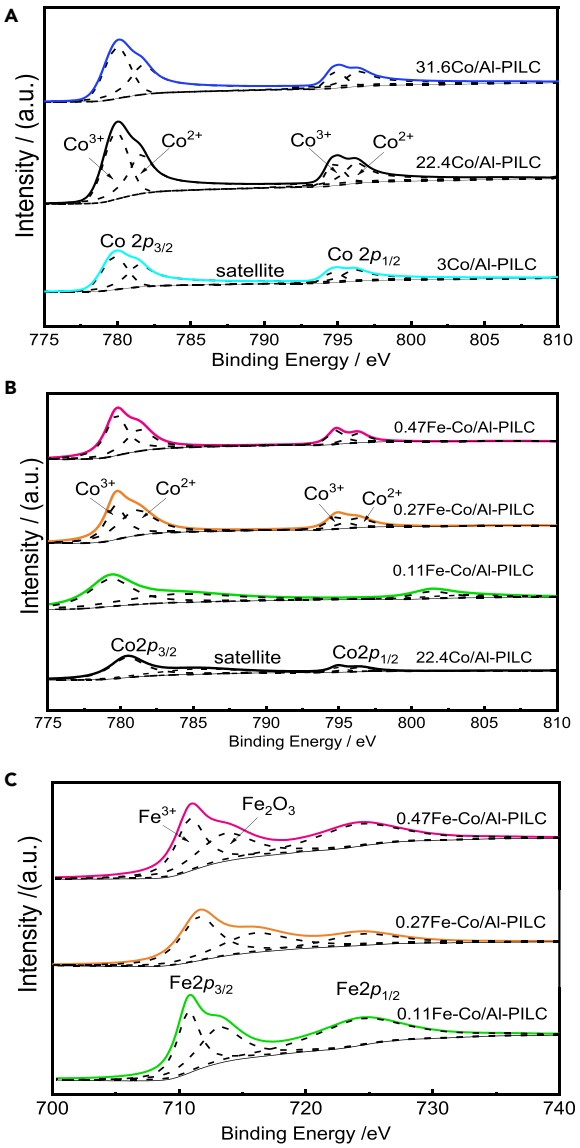

Figure 5. X-ray photoelectron spectrum (XPS) spectra of catalysts

(A) XPS spectra of Co 2*p* of 3Co/Al-PILC, 22.4Co/Al-PILC, and 31.6Co/Al-PILC catalysts.

(B) XPS spectra of Co 2*p* of 22.4Co/Al-PILC, 0.11Fe-Co/Al-PILC, 0.27Fe-Co/Al-PILC, and 0.47Fe-Co/Al-PILC catalysts.

(C) XPS spectra of Fe 2*p* of 0.11Fe-Co/Al-PILC, 0.27Fe-Co/Al-PILC, and 0.47Fe-Co/Al- PILC catalysts.

According to Wen,[7] Figure 5C shows that the chemical state of Fe was Fe^{3+} caused by the presence of Fe 2p1/2 and Fe 2p3/2 that was deconvoluted into two shoulder bands, which appeared at approximately 710.8–711.6 eV and 713.3–716.0 eV, separately. The former was the band of the isolated Fe^{3+}, and the latter belonged to the Fe^{3+} of Fe_2O_3 particles.[39] Previous work indicated that Fe_2O_3 species were conducive to enhancing the complete oxidation of CH_4 by oxygen and unfavorable for the reaction of CH_4-SCR,[34] while the isolated Fe^{3+} promoted the reaction of CH_4 and NO. Among the *x*Fe-Co/Al-PILC catalysts, 0.27Fe-Co/Al-PILC had the lowest Fe_2O_3 species with the highest binding energy of about 711.6 eV and the most content of isolated Fe^{3+}, which was favorable for the NO reduction reaction. Hence, the 0.27 Fe-Co/Al-PILC had the best CH_4-SCR performance. These results indicated that the isolated Fe^{3+} improved the CH_4-SCR performance, while Fe_2O_3 species were conducive to the reaction between CH_4 and O_2. The finding was consistent with the CH_4 conversion in Figure 1B.

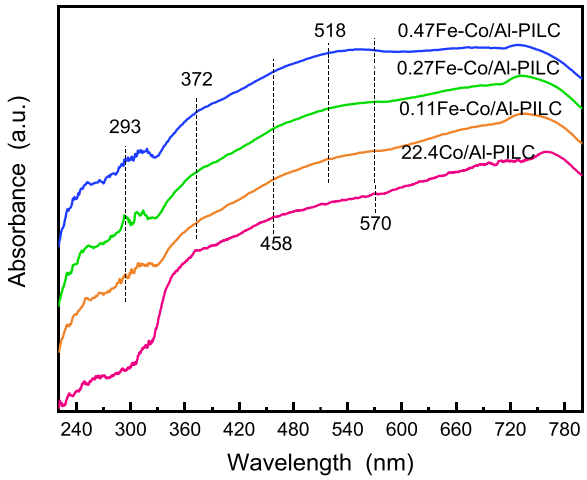

Figure 6. UV-vis spectrum of 22.4Co/Al-PILC, 0.11Fe-Co/Al-PILC, 0.27Fe-Co/Al-PILC, and 0.47Fe-Co/Al-PILC catalysts

UV-vis spectra

Four absorption peaks with different intensities between 370 and 780 nm are shown in Figure 6, mainly reflected on the oxides Co_3O_4 and CoO composed of Co^{2+} and Co^{3+} in the tetrahedron and octahedron.[40] The absorption peak at 458 nm corresponded to Co^{2+} species located in the carrier channel, while the adsorption peak at 570 nm was assigned to Co^{2+} distributed near the six-member ring. After doping ferric, the absorption band at 293 nm emerged in the catalyst spectrum, which may be the change from isolated Fe^{3+} owning a 5 or 6 coordination to Fe^{3+} in the octahedron of the small Fe_xO_y oligomers.[34] Owing to the band between the 300 nm and 400 nm corresponding to Fe_xO_y clusters, the absorption peak at 372 nm was related to the Fe_xO_y oligomers like $[HO-Fe-O-Fe-OH]^{2+}$ species. However, the peaks at 518 nm belonged to the presence of the Fe_2O_3 particles, ascribed to the bands above 400 nm belonged nano-Fe_xO_y species.[7] In addition, the four catalysts all have absorption peaks corresponding to Co^{2+} generated from CoO species at 458 and 570 nm. The results have shown that the prepared catalysts contained some active sites, such as Co^{2+}, CoO species, isolated Fe^{3+}, Fe_xO_y clusters, and Fe_2O_3 particles. Previous works indicated that the isolated Co^{2+},[37] CoO particles, and isolated Fe^{3+} could improve the NO conversion, while the Fe_2O_3 species were conducive to the reaction between CH_4 and O_2, which was unfavorable for the CH_4-SCR. The finding was consistent with the XPS results.

H_2-TPR results

Figure 7 displays the redox performance of the prepared samples explored using the H_2-TPR technique. For the 22.4Co/Al-PILC sample, only one broad reduction peak presented at about 430°C, which belonged to the reduction of CoO to Co[18.] After adding Fe, a new TPR peak appeared at nearly 350°C on the catalysts, which showed that the presence of ferric improved the reducibility of these samples at medium and high temperatures, further improving the catalytic ability. Based on previous studies, the TPR peak at nearly 350°C belonged to the process of Fe^{3+} reducing to Fe^{2+}.[28,29] For the 0.27Fe-Co/Al-PILC sample, the reduction peak of the Fe^{3+} to Fe^{2+} corresponded to the lowest temperature of 327°C, which indicated that the catalyst displayed the best redox ability. It was worth noting that the reduction peak of CoO to Co at around 430°C under the Fe presence atmosphere shifted to a lower temperature, which may be due to the Fe element enhanced the dispersion of cobalt species that were easier to be reduced. In addition, the new peak appeared in the range of 600°C–700°C over *x*Fe-Co/Al-PILC catalysts ascribed to the reduction of Fe_3O_4 to Fe. It was worth noting that the reduction peak of Fe_3O_4 to Fe over the 0.27Fe-Co/Al-PILC catalyst shifted to the lower temperature, which demonstrated that the 0.27Fe-Co/Al-PILC had higher reducibility, which may be a reason for its having the best performance of CH_4-SCR.

Py-FTIR

The nature of acid sites that significantly affect the catalytic activity on the catalyst samples was explored by using the Py-FTIR technology. The infrared spectrum of catalysts treated at 150°C and 300°C is shown in

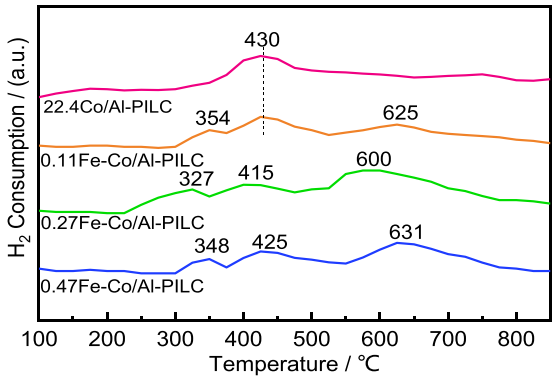

Figure 7. H_2-TPR curves of 22.4Co/Al-PILC, 0.11Fe-Co/Al-PILC, 0.27Fe-Co/Al-PILC, and 0.47Fe-Co/Al-PILC catalysts

Figure 8. Figure 8 displayed that the bands near 1447 and 1608 cm^{-1} attributed to the coordinated pyridine molecules (PyL) due to the coordinatively unsaturated metal cationic sites,[3] while the 1545 cm^{-1} corresponded to the pyridinium ions (PyH^+),[7] which might be generated from the OH-groups.[41] However, the spectral bands at about 1491 and 1638 cm^{-1} corresponded to the PyL+PyH^+ acid complex.[14] These results suggested that the prepared catalysts owned Lewis and Brønsted acid. Noteworthily, the intensity of bands became weak with the desorption temperature increasing.

Table 3 shows the density of Brønsted and Lewis acids. The introduction of ferric caused a drop in Lewis acid levels, while the amount of Lewis acid sites on 0.27Fe-Co/Al-PILC catalysts increased, which may be due to the proper ferric amount could help increase the amount of the unsaturated cationic sites.[7] According to Jung,[42] the Lewis acid could help improve the reaction ratio of the NO for SCR. Besides, the NO absorption main was performed at the Lewis acid sites.[43] Kantcheva also demonstrated that the Lewis acid sites could activate CH_4 to generate the formate species that were the significant intermediates for CH_4-SCR.[44] However, the content of Brønsted acid for the prepared samples was significantly lower than that of Lewis acid. Hence, the study suggested that the Lewis acids were the main active sites of SCR activity, and the Brønsted acid slightly enhanced reactive activity.[45] Therefore, the 0.27Fe-Co/Al-PILC catalyst exhibited the best catalytic performance among the samples.

The significant difference between the Brønsted and Lewis acid levels can be explained by the B/L value, which refers to the ratio of the content of Brønsted to Lewis of one catalyst. Figure 9 displayed that the B/L value over 0.27Fe-Co/Al-PILC catalyst was smaller than the ratio value of the others at 300°C, demonstrating that the Fe to Co of 0.27 can improve the proportion of the Lewis acid sites at a higher temperature. In addition, the B/L values rose with the temperature increasing, which suggested the strength of the Lewis acid sites declined at the higher temperature. The finding was consistent with the result in Figure 8.

In situ DRIFTS

The CH_4-SCR reaction mechanism over the prepared catalysts was investigated by *in situ* DRIFTS technology. Figure 10 presents adsorption DRIFTS spectra over 0.27 Fe-Co/Al-PILC catalyst.

When only NO adsorption at room temperature, five adsorption bands appeared at 1713, 1634, 1557, 1486, and 1310 cm^{-1}, respectively, shown in Figure 10A. The absorption band located at 1713 cm^{-1} was associated with N_2O_4 species caused by adsorbed NO_2 dimerization,[46] and the bridging bidentate nitrates corresponded to the adsorption peak of 1634 cm^{-1}.[47] 1557 cm^{-1} band was caused by the N-O antisymmetric stretching vibration, corresponding to nitrate or NO_2 species.[48] The monodentate nitrates and bridge nitrites were present at 1486 and 1310 cm^{-1}, respectively.[47] Besides, the intensities of the infrared peaks increased with time, indicating that the adsorption capacity of the NO over the 0.27Fe-Co/Al-PILC catalyst was strong as well as the dominant species on the sample surface were the N_2O_4 and monodentate nitrates.

After adding the oxygen, the infrared spectrum exhibited slight changes (Figure 10B). The intensity of the infrared absorption peak related to the N_2O_4 particles (1713 cm^{-1}) increased, which may be due to more

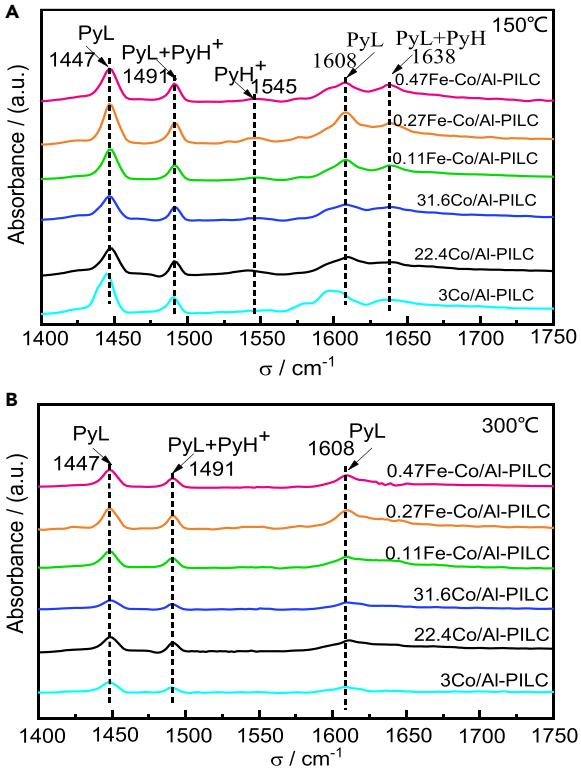

Figure 8. The infrared spectrum of pyridine adsorbed on the prepared catalysts at different temperatures

(A) The infrared spectrum of pyridine adsorption at 150°C.

(B) The infrared spectrum of pyridine adsorption at 300°C.

NO_2 produced dimerized or N_2O_3 being oxidized by oxygen. However, the other intensities of these bands (1634, 1557, 1486, 1310 cm^{-1}) were no intensive changes. Noteworthy, the adsorption peaks at 1604 and 1456 cm^{-1} corresponding to NO_x groups excited at 20 and 30 min when only NO adsorption (Figure 10A), while the adsorption peaks occurred at 1604 and 1456 cm^{-1} at the beginning when adding O_2. The peak at around 1604 cm^{-1} was related to bidentate nitrates (NO_3^-), and the adsorption peak of 1456 cm^{-1} referred to monodentate nitrites related to nitrosyl groups. These results demonstrate that oxygen contributes to the formation of N_2O_4, monodentate nitrates, and monodentate nitrites. The result further indicates that O_2 can accelerate the activation of the NO adsorbed on the isolated cobalt cations sites, and it is easier to form important intermediates (such as NO_2, NO_3^-) that promote the reduction reaction.[49] Relevant studies have shown that intermediates such as NO_2 more easily react with reducing agents than NO to improve the reaction efficiency.[50]

Figure 10C displays the infrared spectra of CH_4 + O_2 adsorption for 30 min at room temperature over the 0.27Fe-Co/Al-PILC sample. Characteristics at 3018 and 1305 cm^{-1} were the gaseous CH_4.[51] The bands at 1660 and 1561cm^{-1} were caused by the stretching vibration of C=O and the COO^- of carboxylates, respectively. Besides, the absorption peak of 1470 cm^{-1} was related to the CH_3 adsorption species, which may be due to the CH_4 adsorbed on Lewis sites could be easily activated on active sites to form a CH_3 group in the absence of NO.[52] The strong Lewis promoted the C-H bond cleave and produced the C-O bond simultaneously. These results indicated that methane molecules attached to the Lewis acid sites were partly activated under the presence of oxygen and in the absence of NO, which was due to the oxygen can decrease the energy of the CH_4 dissociates an H and the subsequent adsorption, indicating that the oxygen significantly enhances the activation and decomposition of methane over the 0.27Fe-Co/Al-PILC.

Figure 10D displayed the spectrum of mixture gas co-adsorption (NO + CH_4 + O_2) at room temperature after introducing the NO. Compared with the profiles exhibited in Figure 10C, a new absorption peak at around 1929 cm^{-1} related to the Co^{2+}-nitrosyl group.[53] Furthermore, the absorption band of the CH_4

Table 3. Brønsted and Lewis acid levels for samples

	150°C		300°C	
Samples	Brønsted (μmol/g)	Lewis (μmol/g)	Brønsted (μmol/g)	Lewis (μmol/g)
22.4Co/Al-PILC	22.51	122.24	16.57	82.10
0.11Fe-Co/Al-PILC	15.72	106.68	12.96	61.76
0.27Fe-Co/Al-PILC	23.84	146.70	15.32	86.43
0.47Fe-Co/Al-PILC	16.45	102.24	14.68	61.59

absorbed on the surface of the 0.27Fe-Co/Al-PILC catalyst occurred at 3018 cm^{-1}. Similarly, the vibration of C-O (1660 cm^{-1}) and the COO^- of carboxylates (1565 cm^{-1}) were also observed. Meanwhile, two new adsorption bands were ascribed to monodentate nitrates that occurred at 1483 and 1298 cm^{-1}.[7] It can be deduced that COO^- of carboxylates and monodentate nitrates are mainly species in the reaction process of CH_4-SCR by comparing the intensities of these adsorption peaks. The emergence of new adsorption bands indicates that nitrogen compounds may be significant reaction intermediates contributing to catalytic activity.

With temperature increasing from 100°C to 500°C, the DRIFTS spectrum of NO + CH_4 + O_2 is exhibited in Figure 10E. The intensity of gaseous CH_4 (3017 cm^{-1}) declined with the temperature increasing. However, the peak intensity of gaseous CO_2 (2349 cm^{-1}) first increased and then decreased. In particular, the peak intensity increased significantly at 300°C and 400°C along with the NO_2 (1627 cm^{-1}) and NO_3^- species (1574 cm^{-1}) peak intensities significantly decreased. The phenomenon indicated that NO_2 and NO_3^- species may be consumed by participating in the reaction of $2NO_2 + CH_4 = N_2 + CO_2 + H_2O$ and $2NO_2 \rightleftharpoons NO_3^- + NO^+$. Meanwhile, those bands decreased and even vanished when the temperature increased to 500°C due to nitrogen-oxo species being easier to react with the methane to form CH_3 radicals and then short-lived nitromethane (CH_3NO_2) at higher temperatures. The finding was consistent with the NO removal ratio rising from 6.8% to 59.4% as the temperature rose from 300°C to 500°C (Figure 1). It was worth noting that the Co^{2+}-nitrosyl group appeared at 1929 cm^{-1} at 30°C shown in Figure 10D, while the band disappeared at 100°C as displayed in Figure 10E. This phenomenon indicated that Co^{2+}-nitrosyl species participated in the catalytic reduction reaction during heating. Besides, the intensities of 1458 cm^{-1} related to the OCO stretching vibration decreased and even vanished at high temperatures, demonstrating that these species were unstable. The infrared absorption peaks that appeared at 1347 and 1304 cm^{-1} are attributed to formate species and gas-phase CH_4 separately. When the temperature was below 400°C, the formate (1347 cm^{-1}) gradually decreased with the temperature and even disappeared at 500°C. This phenomenon showed that all these intermediates participated in the catalytic reaction. Additionally, the CH_4 vibration band at 1304 cm^{-1} indicated methane incompletely participated in the SCR reaction, which also can be deduced from the result in Figure 1B.

Through the *in situ* DRIFTS technology analysis, a preliminary reaction route of CH_4-SCR on 0.27Fe-Co/Al-PILC catalyst is proposed, and the reaction scheme is displayed in Figure 10F. The gaseous methane, nitrous oxide, and oxygen will be adsorbed on the sample surface's active sites. Cobalt oxide species can be the active sites for the NO-converted NO_2 and NO_3^- species. The Lewis acidity and CoO species can contribute to activating the CH_4 to form CH_3 radicals and then further produce the short-lived nitromethane (CH_3NO_2) and the $C_xH_yO_z$ species containing the main intermediate formate species ($HCOO^-$). The next step was the $HCOO^-$ interacted with the NO_3^- (NO_2) to generate the N_2, CO_2, and H_2O. Meanwhile, the CH_3NO_2 interacted with the gaseous NO to generate N_2, CO_2, and H_2O.

Conclusions

Bimetal catalysts based on Fe and Co supported on Al pillared interlayer clays (Fe-Co/Al-PILC) were successfully prepared via the impregnation method. The monometallic and bimetallic systems were characterized, and their catalytic performance for NO_x removal from CH_4-SCR was investigated. The CH_4-SCR results suggested that the Fe and Co bimetal-loaded catalysts exhibited better catalytic activity than the single metal catalyst (Co/Al-PILC) due to the loading of Fe on Al-PILC support can increase the dispersion of active species. Among the prepared catalysts, 0.27Fe-Co/Al-PILC displayed the optimal NO conversion of about 64% at 600°C and 100% of N_2 selectivity due to the doping of Fe being unfavorable for the

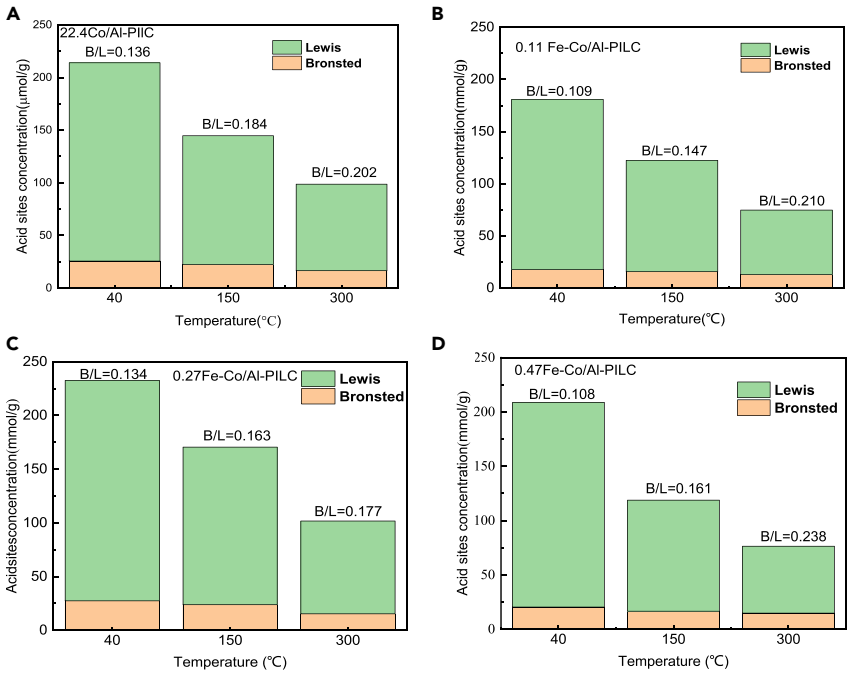

Figure 9. Concentration of surface acid sites of samples

(A) The Lewis and Brønsted acid concentration of 22.4Co/Al-PILC catalyst.

(B) The Lewis and Brønsted acid concentration of 0.11Fe-Co/Al-PILC catalyst.

(C) The Lewis and Brønsted acid concentration of 0.27Fe-Co/Al-PILC catalyst.

(D) The Lewis and Brønsted acid concentration of 0.47Fe-Co/Al-PILC catalyst.

formation of N_2O and NO_2. In addition, an appropriate Fe-Co mass fraction could promote the formation of Co^{2+} attributed to CoO and improve the conversion of NO, as well as improve the H_2O and SO_2 resistance of the *x*Fe-Co/Al-PILC catalysts and enhance the formation of the Lewis acid sites. However, the NO removal efficiency of the 0.47Fe-Co/Al-PILC sample was lower than that of the 0.27Fe-Co/Al-PILC due to Fe_2O_3 particles agglomerating caused the Al-PILC channels generated blocking, excess Fe resulted in generating more Fe_2O_3 particles, which was unfavorable for the reaction of NO with CH_4. Based on the *in situ* DRIFTS experiments, a possible reaction mechanism of CH_4-SCR was proposed. Various nitrates and short-lived nitromethane (CH_3NO_2) were the significant intermediates during the CH_4-SCR reaction. Subsequently, the formed formate species ($HCOO^-$) and CH_3NO_2 were further converted into N_2, CO_2, and H_2O.

Limitations of the study

The modification methods of clays need to be studied in depth. In the paper, a single Al columnar clay modification method is used to prepare Al-PILC carriers loaded with active metals and subsequent research attempts to change the modification method of columnar clays and the type of metal ions. Subsequent studies will try to change the second active metal or add a third active metal to reduce the effective temperature window of the catalyst.

STAR★METHODS

Detailed methods are provided in the online version of this paper and include the following:

- KEY RESOURCES TABLE
- RESOURCE AVAILABILITY
  - Lead contact
  - Materials availability
  - Data and code availability
- EXPERIMENTAL MODEL AND STUDY PARTICIPANT DETAILS

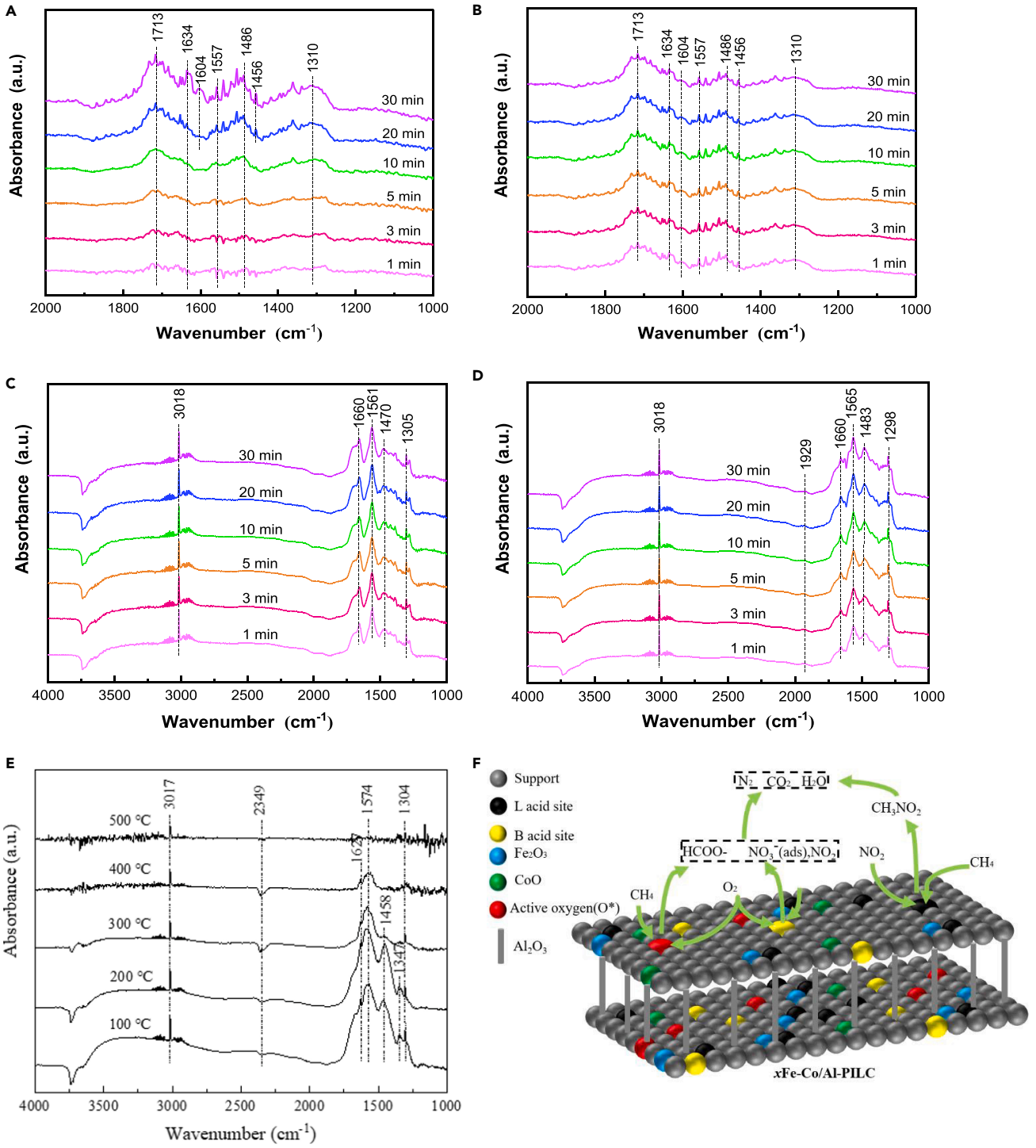

Figure 10. Adsorption DRIFTS spectra over 0.27Fe-Co/Al-PILC catalyst

Conditions: 0.1% NO, 0.2% CH_4, 2% O_2, N_2 balance.

(A) NO adsorption.

(B) NO + O_2 adsorption.

(C) CH_4 + O_2 adsorption.

(D) NO + CH_4 + O_2 adsorption at room temperature.

(E) NO + CH_4 + O_2 heating adsorption from 100°C to 500°C.

(F) Proposed mechanism of the CH_4-SCR reaction.

ACKNOWLEDGMENTS

The work was supported by the National Natural Science Foundation of China (52276103).

AUTHOR CONTRIBUTIONS

S.Y.N.: Investigation, Formal analysis, Writing-original draft. S.S.H.: Investigation, Methodology, Data curation. H.H.Y. and B.T.Z.: Writing-review & editing. Y.X.S: Project administration, Resources, Supervision, Validation.

DECLARATION OF INTERESTS

The authors declare no competing interests.

INCLUSION AND DIVERSITY

We support inclusive, diverse, and equitable conduct of research.

Received: April 4, 2023
Revised: May 5, 2023
Accepted: July 16, 2023
Published: July 20, 2023

REFERENCES

1. Wen, N., Su, Y., Deng, W., Zhou, H., Hu, M., and Zhao, B. (2022). Synergy of CuNiFe-LDH based catalysts for enhancing low-temperature SCR-C_3H_6 performance: surface properties and reaction mechanism. Chem. Eng. J. *438*, 135570. https://doi.org/10.1016/j.cej.2022.135570.

2. Keskin, Z., Özgür, T., Özarslan, H., and Yakaryılmaz, A.C. (2021). Effects of hydrogen addition into liquefied petroleum gas reductant on the activity of Ag-Ti-Cu/Cordierite catalyst for selective catalytic reduction system. Int. J. Hydrogen Energy *46*, 7634–7641. https://doi.org/10.1016/j.ijhydene.2020.11.200.

3. Wen, N., Su, Y., Deng, W., Zhou, H., and Zhao, B. (2021). Selective catalytic reduction of NO with C_3H_6 over CuFe-containing catalysts derived from layered double hydroxides. Fuel *283*, 119296. https://doi.org/10.1016/j.fuel.2020.119296.

4. Zhou, H., Ge, M., Wu, S., Ye, B., and Su, Y. (2018). Iron based monolithic catalysts supported on Al_2O_3, SiO_2, and TiO_2: a comparison for NO reduction with propane. Fuel *220*, 330–338. https://doi.org/10.1016/j.fuel.2018.01.077.

5. Gu, H., Chun, K.M., and Song, S. (2015). The effects of hydrogen on the efficiency of NO_x reduction via hydrocarbon-selective catalytic reduction (HC-SCR) at low temperature using various reductants. Int. J. Hydrogen Energy *40*, 9602–9610. https://doi.org/10.1016/j.ijhydene.2015.05.070.

6. Zhao, J., Li, Z., Zhu, R., Zhang, J., Ding, R., Wen, Z., Zhu, Y., Zhang, G., and Chen, B. (2021). Mechanism of the selective catalytic reduction of NO_x with CH_4 on In/H-beta. Catal. Sci. Technol. *11*, 5050–5061. https://doi.org/10.1039/d1cy00504a.

7. Wen, N., Lin, R., Su, Y., Deng, W., Zhou, H., and Zhao, B. (2021). SCR of NO with CH_4 over Fe/Ga_2O_3-Al_2O_3 and the mechanism. J. Environ. Chem. Eng. *9*, 105014. https://doi.org/10.1016/j.jece.2020.105014.

8. Lim, J.B., Shin, J., Ahn, N.H., Heo, I., and Hong, S.B. (2020). Selective catalytic reduction of NO with CH_4 over cobalt-exchanged cage-based, small-pore zeolites with different framework structures. Appl. Catal. B Environ. *267*, 118710. https://doi.org/10.1016/j.apcatb.2020.118710.

9. Pan, H., Jian, Y., Yu, Y., He, C., Shen, Z., and Liu, H. (2017). Regeneration and sulfur poisoning behavior of In/H-BEA catalyst for NO_x reduction by CH_4. Appl. Surf. Sci. *401*, 120–126. https://doi.org/10.1016/j.apsusc.2016.12.201.

10. Yang, J., Chang, Y., Dai, W., Wu, G., Guan, N., Li, L., and Li, L.D. (2018). Ru-In/H-SSZ-13 for the selective reduction of nitric oxide by methane: insights from temperature-programmed desorption studies. Appl. Catal. B Environ. *236*, 404–412. https://doi.org/10.1016/j.apcatb.2018.05.048.

11. Mendes, A.N., Zholobenko, V.L., Thibault-Starzyk, F., Costa, P.D., and Henriques, C. (2016). On the enhancing effect of Ce in Pd-MOR catalysts for NO_x CH_4-SCR: a structure-reactivity study. Appl. Catal. B Environ. *195*, 121–131. https://doi.org/10.1016/j.apcatb.2016.05.004.

12. Boutros, M., Gálvez, M.E., Onfroy, T., and Da Costa, P. (2014). Influence of synthesis parameters of SBA-15 supported palladium catalysts for methane combustion and simultaneous NO_x reduction. Micropor. Mesopor. Mater. *183*, 1–8. https://doi.org/10.1016/j.micromeso.2013.08.031.

13. Teng, Z., Zhang, H., Huang, S., Li, N., and Zhou, Q. (2018). Experimental study on reduction of NO by CH_4 over $La_{0.8}Sr_{0.2}MnO_3$/alpha-Al_2O_3 in excess of O^{-2}. J. Taiwan Inst. Chem. Eng. *87*, 204–210. https://doi.org/10.1016/j.jtice.2018.03.036.

14. Takahashi, M., Inoue, N., Nakatani, T., Takeguchi, T., Iwamoto, S., Watanabe, T., and Inoue, M. (2006). Selective catalytic reduction of NO with methane on gamma-Ga_2O_3-Al_2O_3 solid solutions prepared by the glycothermal method. Appl. Catal. B Environ. *65*, 142–149. https://doi.org/10.1016/j.apcatb.2006.01.007.

15. Resini, C., Montanari, T., Nappi, L., Bagnasco, G., Turco, M., Busca, G., Bregani, F., Notaro, M., and Rocchini, G. (2003). Selective catalytic reduction of NO_x by methane over Co-H-MFI and Co-H-FER zeolite catalysts: characterisation and catalytic activity. J. Catal. *214*, 179–190. https://doi.org/10.1016/s0021-9517(02)00153-7.

16. Lónyi, F., Solt, H.E., Pászti, Z., and Valyon, J. (2014). Mechanism of NO-SCR by methane over Co,H-ZSM-5 and Co,H-mordenite catalysts. Appl. Catal. B Environ. *150–151*, 218–229. https://doi.org/10.1016/j.apcatb.2013.12.024.

17. Gil, B., Janas, J., Włoch, E., Olejniczak, Z., Datka, J., and Sulikowski, B. (2008). The influence of the initial acidity of HFER on the status of Co species and catalytic performance of CoFER and InCoFER in CH_4-SCR-NO. Catal. Today. *137*, 174–178. https://doi.org/10.1016/j.cattod.2008.01.004.

18. Lónyi, F., Solt, H.E., Valyon, J., Boix, A., and Gutierrez, L.B. (2012). The SCR of NO with methane over In,H- and Co,In,H-ZSM-5 catalysts: The promotional effect of cobalt. Appl. Catal. B Environ. *117–118*, 212–223. https://doi.org/10.1016/j.apcatb.2012.01.022.

19. Tian, F., Li, K., and Su, Y. (2020). Catalytic performance and characterization of Ce-modified Fe catalysts supported on Al_2O_3 for SCR-C_3H_8. Catal. Surv. Asia *24*, 239–249. https://doi.org/10.1007/s10563-020-09306-4.

20. Su, Y., Zhao, B., and Deng, W. (2016). Removal of NO by methane over iron in simulated flue gas with SO_2. Fuel *170*, 9–15. https://doi.org/10.1016/j.fuel.2015.12.021.

21. Dong, S.L., Su, Y.X., Liu, X., Li, Q.C., Yuan, M.H., Zhou, H., and Deng, W.Y. (2018). Experimental study on selective catalytic reduction of NO by C_3H_6 over Fe/Ti-PILC catalysts. J. Fuel Chem. Technol. *46*, 1231–1239. https://doi.org/10.1016/S1872-5813(18)30051-3.

22. Li, Q.C., Su, Y.X., Dong, S.L., Yuan, M.H., Zhou, H., and Deng, W.Y. (2018). Fe-PILC for selective catalytic reduction of NO by propene under lean-burn conditions. J. Fuel Chem. Technol. *46*, 1240–1248.

23. Zhang, X.W., Su, Y.X., Cheng, J.H., Lin, R., Wen, N.N., Deng, W.Y., and Zhou, H. (2019). Effect of Ag on deNO_x performance of SCR-C_3H_6 over Fe/Al-PILC catalysts. J. Fuel Chem. Technol. *47*, 1368–1378. https://doi.org/10.1016/S1872-5813(19)30055-6.

24. Mnasri-Ghnimi, S., and Frini-Srasra, N. (2019). Removal of heavy metals from aqueous solutions by adsorption using single and mixed pillared clays. Appl. Clay Sci. *179*, 105151. https://doi.org/10.1016/j.clay.2019.105151.

25. Candan Karaeyvaz, M., and Balci, S. (2021). One pot synthesis of aluminum pillared intercalated layered clay supported silicotungstic acid (STA/Al-PILC) catalysts. Micropor. Mesopor. Mater. *323*, 111193. https://doi.org/10.1016/j.micromeso.2021.111193.

26. Zuo, S., Yang, P., and Wang, X. (2017). Efficient and environmentally friendly synthesis of AlFe-PILC supported MnCe catalysts for benzene combustion. ACS Omega *2*, 5179–5186. https://doi.org/10.1021/acsomega.7b00592.

27. Mrad, R., Cousin, R., Poupin, C., Aboukaïs, A., and Siffert, S. (2015). Propene oxidation and NO reduction over MgCu-Al(Fe) mixed oxides derived from hydrotalcite-like compounds. Catal. Today *257*, 98–103. https://doi.org/10.1016/j.cattod.2015.02.020.

28. Martínez-Hernández, A., Fuentes, G.A., and Gómez, S.A. (2015). Selective catalytic reduction of NO_x with C_3H_8 using Co-ZSM5 and Co-MOR as catalysts: A model to account for the irreversible deactivation promoted by H_2O. Appl. Catal. B Environ. *166–167*, 465–474. https://doi.org/10.1016/j.apcatb.2014.11.059.

29. Li, B., Zhang, H.Y., Zheng, J.J., Qin, B., Pan, M., Chen, J.Q., Yu, F., Wang, G.S., and Li, R.F. (2015). Bi-phase Zeolites Composite MFI/BEA: Synthesis and Application in Selective Catalytic Reduction of NO_x by Methane. Chin. J. Inorg. Chem. *31*, 1563–1570. https://doi.org/10.11862/cjic.2015.206.

30. Miyahara, Y., Takahashi, M., Masuda, T., Imamura, S., Kanai, H., Iwamoto, S., Watanabe, T., and Inoue, M. (2008). Selective catalytic reduction of NO with C1-C3 reductants over solvothermally prepared Ga_2O_3-Al_2O_3 catalysts: Effects of water vapor and hydrocarbon uptake. Appl. Catal. B Environ. *84*, 289–296. https://doi.org/10.1016/j.apcatb.2008.04.005.

31. Xue, T., Li, R., Gao, Y., and Wang, Q. (2020). Iron mesh-supported vertically aligned Co-Fe layered double oxide as a novel monolithic catalyst for catalytic oxidation of toluene. Chem. Eng. J. *384*, 123284. https://doi.org/10.1016/j.cej.2019.123284.

32. Smeets, P.J., Meng, Q., Corthals, S., Leeman, H., and Schoonheydt, R.A. (2008). Co-ZSM-5 catalysts in the decomposition of N_2O and the SCR of NO with CH_4: Influence of preparation method and cobalt loading. Appl. Cataly. B Environ. *84*, 505–513. https://doi.org/10.1016/j.apcatb.2008.05.002.

33. Thommes, M., Kaneko, K., Neimark, A.V., Olivier, J.P., Rodriguez-Reinoso, F., Rouquerol, J., and Sing, K.S. (2015). Physisorption of gases, with special reference to the evaluation of surface area and pore size distribution (IUPAC Technical Report). Pure Appl. Chem. *87*, 1051–1069. https://doi.org/10.1515/pac-2014-1117.

34. Li, Y., and Armor, J.N. (1993). Selective catalytic reduction of NO_x with methane over metal exchanged zeolites. Appl. Catal. B Environ. *2*, 239–256. https://doi.org/10.1016/0926-3373(93)80051-e.

35. Zhang, H., Li, N., Li, L., Wang, A., Wang, X., and Zhang, T. (2011). Selective catalytic reduction of NO with CH_4 over In-Fe/sulfated zirconia catalysts. Catal. Lett. *141*, 1491–1497. https://doi.org/10.1007/s10562-011-0681-4.

36. Kwak, J.H., Tonkyn, R.G., Kim, D.H., Szanyi, J., and Peden, C.H. (2010). Excellent activity and selectivity of Cu-SSZ-13 in the selective catalytic reduction of NO_x with NH_3. J. Catal. *275*, 187–190. https://doi.org/10.1016/j.jcat.2010.07.031.

37. Wang, X., Chen, H.Y., and Sachtler, W.M.H. (2000). Catalytic reduction of NO_x by hydrocarbons over Co/ZSM-5 catalysts prepared with different methods. Appl. Catal. B Environ. *26*, L227–L239. https://doi.org/10.1016/s0926-3373(00)00125-9.

38. Qi, G., and Yang, R.T. (2005). Selective catalytic oxidation (SCO) of ammonia to nitrogen over Fe/ZSM-5 catalysts. Appl. Catal. A Gen. *287*, 25–33. https://doi.org/10.1016/j.apcata.2005.03.006.

39. Yang, S., Guo, Y., Yan, N., Wu, D., He, H., Xie, J., Qu, Z., and Jia, J. (2011). Remarkable effect of the incorporation of titanium on the catalytic activity and SO_2 poisoning resistance of magnetic Mn-Fe spinel for elemental mercury capture. Appl. Catal. B Environ. *101*, 698–708. https://doi.org/10.1016/j.apcatb.2010.11.012.

40. Chupin, C., Vanveen, A., Konduru, M., Despres, J., and Mirodatos, C. (2006). Identity and location of active species for NO reduction by CH_4 over Co-ZSM-5. J. Catal. *241*, 103–114. https://doi.org/10.1016/j.jcat.2006.04.025.

41. Zaki, M.I., Hasan, M.A., Al-Sagheer, F.A., and Pasupulety, L. (2001). In situ FTIR spectra of pyridine adsorbed on SiO_2-Al_2O_3, TiO_2, ZrO_2 and CeO_2: general considerations for the identification of acid sites on surfaces of finely divided metal oxides. Colloids Surf. A *190*, 261–274. https://doi.org/10.1016/s0927-7757(01)00690-2.

42. Jung, S.M., and Grange, P. (2002). TiO_2-SiO_2 mixed oxide modified with H_2SO_4II. Acid properties and their SCR reactivity. Appl. Catal. A Gen. *228*, 65–73. https://doi.org/10.1016/s0926-860x(01)00960-7.

43. Wang, Y., Lei, Z., Chen, B., Guo, Q., and Liu, N. (2010). Adsorption of NO and N_2O on Fe-BEA and H-BEA zeolites. Appl. Surf. Sci. *256*, 4042–4047. https://doi.org/10.1016/j.apsusc.2010.01.075.

44. Kantcheva, M., and Vakkasoglu, A.S. (2004). Cobalt supported on zirconia and sulfated zirconia I. FT-IR spectroscopic characterization of the NO_x species formed upon NO adsorption and NO/O-2 coadsorption. J. Catal. *223*, 352–363. https://doi.org/10.1016/j.jcat.2004.02.007.

45. Yang, R.T., and Li, W.B. (1995). Ion-exchanged pillared clays- a new calass of catalysts for selective catalytic reduction of NO by hydrocarbons and by ammonia. J. Catal. *155*, 414–417. https://doi.org/10.1006/jcat.1995.1223.

46. Yuan, M., Su, Y., Deng, W., and Zhou, H. (2019). Porous clay heterostructures (PCHs) modified with copper ferrite spinel as catalyst for SCR of NO with C_3H_6. Chem. Eng. J. *375*, 122091. https://doi.org/10.1016/j.cej.2019.122091.

47. Emeis, C.A. (1993). Determination of integrated molar extinction coefficients for infrared-absorption bands of pyridine adsorbed on solid acid catalysts. J. Catal. *141*, 347–354. https://doi.org/10.1006/jcat.1993.1145.

48. Richter, M., Trunschke, A., Bentrup, U., Brzezinka, K.W., Schreier, E., Schneider, M., Pohl, M.M., and Fricke, R. (2002). Selective catalytic reduction of nitric oxide by ammonia over egg-shell MnO_x/NaY composite catalysts. J. Catal. *206*, 98–113. https://doi.org/10.1006/jcat.2001.3468.

49. Ren, X., Tan, H., Jie, Q., and Liu, J. (2020). DFT studies of the CH_4-SCR of NO on Fe-doped $ZnAl_2O_4$(100) surface under oxygen conditions. RSC Adv. *11*, 927–933. https://doi.org/10.1039/d0ra10017j.

50. Liu, J., Li, X., Zhao, Q., Hao, C., and Zhang, D. (2013). Insight into the mechanism of selective catalytic reduction of NO_x by propene over the $Cu/Ti_{0.7}Zr_{0.3}O_2$ catalyst by fourier transform infrared spectroscopy and density functional theory calculations. Environ. Sci. Technol. *47*, 4528–4535. https://doi.org/10.1021/es3049898.

51. Shi, Y., Pu, J., Gao, L., and Shan, S. (2021). Selective catalytic reduction of NO_x with NH_3 and CH_4 over zeolite supported indium-cerium bimetallic catalysts for lean-burn natural gas engines. Chem. Eng. J. *403*, 126394. https://doi.org/10.1016/j.cej.2020.126394.

52. Gao, E., Pan, H., Wang, L., Shi, Y., and Chen, J. (2020). Identification of main active sites and the role of NO_2 on NO_x reduction with CH_4 over In/BEA catalyst: a computational study. Catalysts *10*, 572. https://doi.org/10.3390/catal10050572.

53. Lobree, L.J., Aylor, A.W., Reimer, J.A., and Bell, A.T. (1997). Role of cyanide species in the reduction of NO by CH_4 over Co-ZSM-5. J. Catal. *169*, 188–193. https://doi.org/10.1006/jcat.1997.1699.

STAR★METHODS

KEY RESOURCES TABLE

REAGENT or RESOURCE	SOURCE	IDENTIFIER
Chemicals, peptides, and recombinant proteins		
Sodium hydroxide	Sinopharm Chemical Regent Co. Ltd	CAS#:1310-73-2
Aluminum chloride hexahydrate	Sinopharm Chemical Regent Co. Ltd	CAS#:7784-13-6
Montmorillonite	Sinopharm Chemical Regent Co. Ltd	CAS#:1318-93-0
Iron(III) nitrate nonahydrate	Sinopharm Chemical Regent Co. Ltd	CAS#:7782-61-8
Cobalt nitrate hexahydrate	Sinopharm Chemical Regent Co. Ltd	CAS#:10026-22-9
Nitrogen monoxide	Dalian Special Gases Co. Ltd	N/A
Methane	Dalian Special Gases Co. Ltd	N/A
Oxygen	Dalian Special Gases Co. Ltd	N/A
Nitrogen	Dalian Special Gases Co. Ltd	N/A
Sulphur dioxide	Shanghai Wetry Standard Reference Gas Analytical Technology Co. Ltd	N/A
Software and algorithms		
Origin	OriginLab	www.originlab.com
Avantage	Thermo Avantage	www.surfsciftp.co.uk/avant5/
Other		
Inductively coupled plasma, ICP	Leeman	Prodigy-ICP; www.instrument.com.cn/pic/C135980.html
X-ray Diffractometer, XRD	Rigaku	D/MAX-2200; https://www.rigaku.com/products/xrd
X-ray photoelectron spectrum, XPS	Thermo Fisher	Escalab 250 Xi; http://www.labbase.net/Product/ProductItems-21-10-802-49971.html
Micromeritics ASAP 2460 analyzer	Micromeritics	ASAP 2460; https://www.chem17.com/st465/product_33854677.html
Ultraviolet–visibility spectroscopy, UV-Vis	Shimadzu	UV 3600 plus; https://www.hbzhan.com/st658831/product_23376994.html
Infrared Fourier Transform Spectroscopy, DRIFTS	Thermo	Nicolet IS50; https://ibook.antpedia.com/p/64374.html
Fourier transforms infrared spectroscopy, FTIR	PerkinElmer	Frontier FT-IR; https://chem.washington.edu/instruments/perkin-elmer-frontier-ftir
Gas chromatograph analyzer	EWAI	GC-4000A; http://www.cn-senbe.com/pddetailthree/product/detail-21331924.html

RESOURCE AVAILABILITY

Lead contact

Further information and requests for resources and reagents should be directed to and will be fulfilled by the lead contact, Yaxin Su (suyx@dhu.edu.cn).

Materials availability

This study did not generate new unique reagents.

Data and code availability

- Data reported in this paper will be shared by the lead contact upon request.
- This paper does not report original code.

- Any additional information required to reanalyze the data reported in this paper is available from the lead contact upon request.

EXPERIMENTAL MODEL AND STUDY PARTICIPANT DETAILS

This study does not use experimental models.

METHOD DETAILS

Chemicals and materials

Sodium hydroxide, aluminum chloride hexahydrate, montmorillonite, Iron(III) nitrate nonahydrate, and cobalt nitrate hexahydrate were all provided by Sinopharm Chemical Regent Co. Ltd (Shanghai, China). Nitrogen monoxide, methane, oxygen, and nitrogen were all purchased from Dalian Special Gases Co. Ltd (Dalian, China). Sulphur dioxide was supplied by Shanghai Wetry Standard Reference Gas Analytical Technology Co. Ltd (Shanghai, China).

Preparation of catalyst

The NaOH solution of 0.4 mol/L was dropped slowly into the rapidly stirred 0.2 mol/L $AlCl_3$ solutions to obtain the aluminum hydroxy-oligomeric solution. The obtained solution was under vigorous stirring for 2 hours at 80°C, where it was left to age at ambient temperature for 24 hours to prepare the aluminum column agent. Then add it to a montmorillonite suspension with a mass fraction of 1% and a pre-stirred 24 hours, making the ratio of Al^{3+}/clay 10 mmol/g. Subsequently, the prepared sample was stirred for 2 hours, aged for 48 hours at 60°C, washed with deionized water until Cl^-free, then dried for 12 hours at 100°C and roasted for 4 hours at 550°C to obtain the Al-PILC carrier.

The above-mentioned Al-PILC support (1 g) was immersed in various concentrations of cobalt nitrate solution. Subsequently, the samples were sonicated at ambient temperature for 4 hours and evaporated for 12 hours at 100°C. Follow calcining at 500°C for 4 hours. The prepared product was denoted as Co/Al-PILC, which was then immersed in different concentrations of ferric nitrate solution to load Fe. Finally, the sample was sonicated at ambient temperature for 4 hours, evaporated at 100°C for 12 hours, and roasted at 550°C for 4 hours. The final production was expressed as the *x*Fe-Co/Al-PILC (*x* refers to the mass fraction of Fe/Co, x = 0.11, 0.27, 0.47).

Catalyst characterization

The Prodigy- inductively coupled plasma (ICP) devise (Leeman, USA) was used to determine the element loading of the prepared samples, and the crystallinity was collected by an X-ray diffractometer (XRD, Rigaku, Japan) furnished with Cu Kα (λ=0.15406 nm). The chemical valence of sample elements was obtained using an X-ray photoelectron spectrum (XPS) collected from Thermo Fisher with an excitation source of Al-Kα (1486.6 eV, 150 W). The N_2 isotherms of catalysts were measured by using Micromeritics ASAP 2460 analyzer (Micromeritics, USA). The BET (Brunauer-Emmett-Teller) procedure and the BJH (Barrett-Joyner-Halenda) method were utilized to characterize the morphology of catalysts, such as surface area and pore size. In addition, the UV-Visibility Spectrometer (UV 3600 plus, Shimadzu, Japan), which is assigned a detection range of 200-800 nm, was used to transmit the UV-Visibility Spectrum.

The reduction performance of the samples was texted using temperature-programmed reduction with hydrogen (H_2-TPR) operated on the gas chromatograph analyzer GC-4000A (EWAI, China) with a thermal conductivity detector (TCD). The catalyst sample of 100 mg was placed in an N_2 atmosphere, pretreated at 300°C for 0.5 hours, and then cooled to ambient temperature. Subsequently, the 100 mg sample was treated with a mixed stream of N_2/H_2(5%H_2 and 95%N_2). The amount of H_2 consumption was recorded every 15°C using the TCD apparatus during heating when the catalyst was heated at a 5°C/min heating rate. Pyridine-adsorption Fourier transforms infrared spectroscopy (Py-FTIR) test was performed on an FTIR Frontier (Frontier FT-IR, USA) to investigate the density of acid sites of the prepared sample. Before testing, the prepared catalyst will be pretreated for 120 min at 500°C. Adsorption of pyridine was performed at room temperature, followed by desorption was operated at vacuum conditions of 40, 150, and 300°C, respectively.

Catalytic activity tests

The activity of the prepared catalyst was performed on a fixed-bed microreactor with an 8mm quartz tube in diameter. 400 mg of catalyst is required for each activity test. Before testing, catalysts were pretreated in the presence of N_2 at 300°C for 30 min, followed by cooling to ambient temperature, and the mixture stream was fed into the fixed-bed microreactor at a flow rate of 200 ml/min, equivalent to GHSV of 14000 h^{-1}. The mixture stream contains NO, CH_4, O_2, SO_2 (when needed), H_2O (when used), and N_2 as balance. The concentration of NO, NO_2, and NO_x was measured through the flue gas analyzer ECOM-J2KN provided with electrochemical sensors, while the amount of N_2 was recorded through chromatograph GC-4000A. The content of CH_4 was measured by a flame ionization detector (FID), and the following equations were used to calculate the NO and CH_4 conversion and N_2 selectivity.

$$NO\ conversion = \frac{[NO]_{in} - [NO]_{out}}{[NO]_{in}} \times 100\% \quad \text{(Equation 1)}$$

$$CH_4\ conversion = \frac{[CH_4]_{in} - [CH_4]_{out}}{[CH_4]_{in}} \quad \text{(Equation 2)}$$

$$S_{N_2} = \frac{[NO]_{in} - [NO]_{out} - [NO_2]_{out} - 2[N_2O]_{out}}{[NO]_{in} - [NO]_{out}} \times 100\% \quad \text{(Equation 3)}$$

In situ DRIFTS

The reaction mechanism of NO reduction for CH_4-SCR was analyzed by monitoring the intermediates using the *in situ* Diffuse Reflectance Infrared Fourier Transform Spectroscopy (*in situ* DRIFTS). The DRIFTS measurements are operated with a spectrometer (Thermo Nicolet IS50). The spectra were detected through a mercury cadmium telluride detector at a scanning resolution of 4 cm^{-1} with an average of 64 scans. Before testing, catalysts were pretreated in the presence of N_2 at 500°C for 3 hours to remove impurities from the sample surface. Precisely control the flow of reaction gases with a mass flow meter. The flow rate of the mixture gas was 20 ml/min.

QUANTIFICATION AND STATISTICAL ANALYSIS

This study use Origin and Avantage for statistical analysis or quantification. The statistical details of experiments are available from the lead contact upon request.

ADDITIONAL RESOURCES

This study has not generated or contributed to a new website/forum.